Frontiers of Information Technology & Electronic Engineering
www.zju.edu.cn/jzus; engineering.cae.cn; www.springerlink.com
ISSN 2095-9184 (print); ISSN 2095-9230 (online)
E-mail: jzus@zju.edu.cn

Moving target detection in the cepstrum domain for passive coherent location (PCL) radar

Ji-chuan LI[†1,3], Xiao-de LU[1], Hui ZHANG[2,3], Peng-cheng YANG[1,3], Yu LIU[1,3], Mao-sheng XIANG[1]

([1]*Science and Technology on Microwave Imaging Laboratory, Institute of Electronics, Chinese Academy of Sciences, Beijing 100190, China*)

([2]*Key Laboratory of Technology in Geo-spatial Information Processing and Application System, Institute of Electronics, Chinese Academy of Sciences, Beijing 100190, China*)

([3]*University of Chinese Academy of Sciences, Beijing 100049, China*)

[†]E-mail: lijichuan10@sina.com

Received Feb. 1, 2015; Revision accepted May 21, 2015; Crosschecked July 8, 2015

Abstract: A cepstrum moving target detection (CEPMTD) algorithm based on cepstrum techniques is proposed for passive coherent location (PCL) radar systems. The primary cepstrum techniques are of great success in recognizing the arrival times of static target echoes. To estimate the Doppler frequencies of moving targets, we divide the radar data into a large number of segments, and reformat these segments into a detection matrix. Applying the cepstrum and the Fourier transform to the fast and slow time dimensions respectively, we can obtain the range information and Doppler information of the moving targets. Based on the CEPMTD outlined above, an improved CEPMTD algorithm is proposed to improve the detection performance. Theoretical analyses show that only the target's peak can be coherently added. The performance of the improved CEPMTD is initially validated by simulations, and then by experiments. The simulation results show that the detection performance of the improved CEPMTD algorithm is 13.3 dB better than that of the CEPMTD algorithm and 6.4 dB better than that of the classical detection algorithm based on the radar cross ambiguity function (CAF). The experiment results show that the detection performance of the improved CEPMTD algorithm is 1.63 dB better than that of the radar CAF.

Key words: Moving target detection, Cepstrum techniques, Cross ambiguity function (CAF), Passive coherent location (PCL) radar

doi:10.1631/FITEE.1500036 **Document code:** A **CLC number:** TN95

1 Introduction

The passive coherent location (PCL) radar systems, operating with transmitters of opportunity, were originally designed for other purposes, such as the global system for mobile communication (GSM), Global Positioning System (GPS), and television broadcasting (Olivadese *et al.*, 2013; Palmer *et al.*, 2013). As illustrated in Fig. 1, there are two receiving channels in the PCL radar system, named the surveillance channel and the reference channel. The surveillance channel receives the target echo signal, while the reference channel receives the reference signal. The classical moving target detection method is the radar cross ambiguity function (CAF) calculated with the reference signal and the target echoes (Sinsky and Wang, 1974; Axelsson, 2004; Yan *et al.*, 2013). However, there is one limitation to the peak sidelobe level (PSL) in radar CAF, which is a fixed value obtained from the product of the time interval and bandwidth of the signal (time-bandwidth product) (Cherniakov, 2008).

In this paper, a cepstrum moving target detection (CEPMTD) algorithm based on cepstrum techniques is proposed for PCL radar systems, which is, to the best of our knowledge, the first attempt to detect moving targets with cepstrum techniques. Andric *et al.*

ORCID: Ji-chuan LI, http://orcid.org/0000-0003-0314-4475

(2011) introduced cepstrum techniques to analyze the radar Doppler signal and identified the different classes of targets by analyzing their cepstrum coefficients. The proposed CEPMTD algorithm can also obtain the accurate Doppler frequency information and the range information of moving targets.

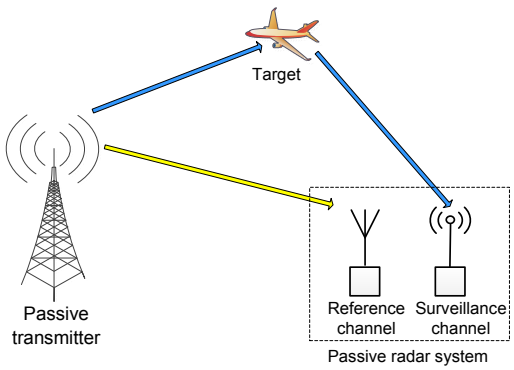

Fig. 1 Block diagram of a passive coherent location radar system

Cepstrum techniques have been widely used for signal detection and extraction in radar and sonar, speech, seismology, etc. (Oppenheim and Schafer, 2004), since the first cepstrum technique was proposed by Bogert *et al.* (1963). Given a signal that is a finite summation of a basic wave and its echoes, applications of cepstrum techniques include the recognition of echo arrival times and the estimation of the wave shape of the basic wave or its echoes (Kemerait and Childers, 1972). There are two main cepstrum techniques, i.e., power cepstrum and complex cepstrum. The most successful application of the power cepstrum is for echo detection (Noll, 1964; 1967), and the greatest successful application of the complex cepstrum is signal separation and recovery (Oppenheim, 1965; Schafer, 1969; Ulrych, 1971; Stoffa *et al.*, 1974).

The procedures of the proposed CEPMTD algorithm are as follows. The target echo signal is weighted by a coefficient and added to the reference signal to obtain a composited signal. The one-dimensional composited radar data are reformatted to be a detection matrix with the fast and slow time dimensions. After applying the cepstrum and the Fourier transform to the fast and slow time dimensions respectively, the range information and Doppler information of the moving targets are obtained by detecting the peaks' positions in the detection matrix surface. In addition, an improved CEPMTD algorithm is proposed to improve the detection capacity. Compared with radar CAF, the detection performance of the improved CEPMTD is better when there is no noise in the radar data, which is validated by simulation results. The detection performance of the improved CEPMTD algorithm is the same as that of the radar CAF when the signal-to-noise ratio (SNR) is low. The experimental results show that the detection performance is 1.63 dB better than that of the radar CAF, which results from the residual of the clutters in the real radar data after clutter removal.

2 Power and complex cepstrums

Block diagrams of the computation of the cepstrums including the power and complex cepstrums are illustrated in Fig. 2.

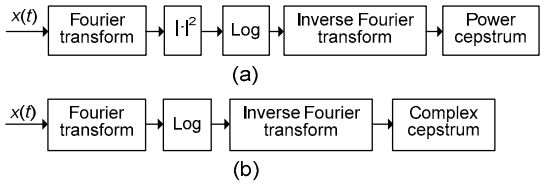

Fig. 2 Block diagrams of power (a) and complex (b) cepstrums

The definition and properties of the power and complex cepstrums are referred to Bogert *et al.* (1963) and Oppenheim (1965), respectively. The power cepstrum is the inverse Fourier transform of the logarithm of the power spectrum of the signal. The complex cepstrum is defined as the inverse Fourier transform of the logarithm of the Fourier transform of the signal.

The applications of the power cepstrum and complex cepstrum have been explored in a variety of fields, including audio processing, speech processing, geophysics radar, and medical imaging (Kim and Rose, 2003; 2009; Hansson-Sandsten and Axmon, 2007; Tsai and Lin, 2011). The applications can be classified into two groups. One is echo detection, and the other is signal separation or recovery. There are many other innovations and applications that can be traced to the cepstrums and their subsequent developments. The readers who are interested in these

applications should refer to Oppenheim and Schafer (2004). Due to the superior detection capability of power cepstrums compared with complex cepstrums (Kemerait and Childers, 1972), we focus on the power cepstrum technique in the following discussion.

3 Moving target detection algorithm: CEPMTD

In this section, a moving detection algorithm, CEPMTD, is proposed for PCL radar. Fig. 3 shows the block diagram of the CEPMTD algorithm. Initially, the target echo signal is weighted by a coefficient and added to the reference signal to obtain a composited signal. As illustrated in Fig. 4, the composited data should be equally segmented into a number of segments. Let N and M represent the numbers of signal sampling points and segments respectively, and D the length of each segment. The detection matrix is constructed by all segments. The row of the detection matrix is named the fast time dimension, while the column is the slow time dimension.

Power cepstrum computation is implemented in the fast time dimension, after which the discrete Fourier transform (DFT) is calculated in the slow time dimension. The moving targets will show up as the noticeable peaks in the detection matrix surface. The positions of the peaks represent the range information and Doppler information of the moving targets.

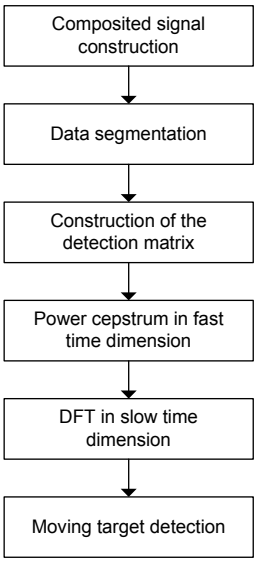

Fig. 3 Block diagram of the CEPMTD algorithm

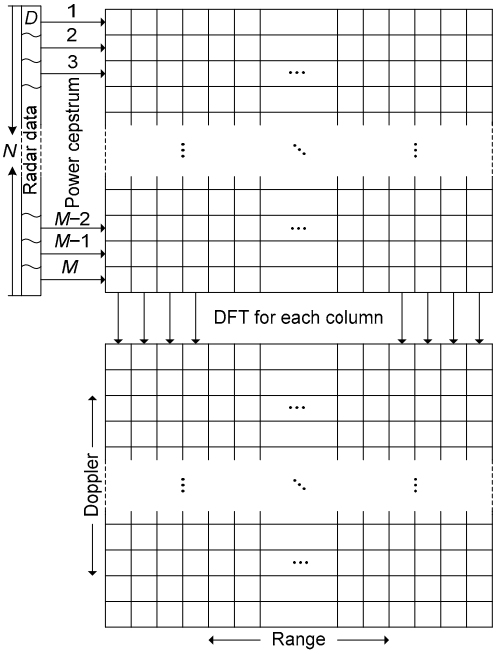

Fig. 4 Signal flow diagram of the detection algorithm

3.1 Data segmentation

In the computation of the CEPMTD algorithm, the radar data need to be equally divided into a number of segments. The length of each segment is closely related to the sampling rate (f_s) and the Doppler observation width (f_d), which is the sampling rate in the slow time dimension. The signal duration is denoted by T_s, which can be obtained from dividing the number of signal sampling points by the sampling rate or from dividing the number of segments by the sampling rate in the slow time dimension:

$$T_s = \frac{N}{f_s} = \frac{M}{f_d}. \tag{1}$$

The length of each segment (D) is obtained from dividing the number of signal sampling points by the number of segments, which can be written as

$$D = \frac{N}{M} = \frac{f_s}{f_d}. \tag{2}$$

When the sampling rate (f_s) is fixed, there is an inverse proportional relationship between the length of each segment and the Doppler observation width.

The resolution of the Doppler frequency is represented as Eq. (3). It is the reciprocal of the signal duration, which is the same as that of the radar CAF (Thomas *et al.*, 2006; Cherniakov, 2008).

$$\Delta f = \frac{f_{\mathrm{d}}}{M} = \frac{1}{T_{\mathrm{s}}}. \tag{3}$$

3.2 Power cepstrum of a single moving target

After data segmentation, each segment constitutes one row of the detection matrix. The power cepstrum of each row should be calculated. The expression of the signal with a single moving target echo can be written as follows:

$$x(n) = s(n) + as(n-l)\mathrm{e}^{\mathrm{j}\omega_{\mathrm{d}} n}, \tag{4}$$

where $s(n)$ denotes the reference signal, $x(n)$ is the composited data containing $s(n)$ and one echo with amplitude a, time delay l, and normalized Doppler frequency ω_{d}. For simplicity, suppose that the Doppler frequency is so small that the Doppler phase is constant within one segment. So, we replace the variable, n, in the superscript of the exponential term in Eq. (4), with a constant, m, which is the beginning time of each segment. Then Eq. (4) is rewritten as

$$x_m(n) = s_m(n) + as_m(n-l)\mathrm{e}^{\mathrm{j}\omega_{\mathrm{d}} m}. \tag{5}$$

Using the notation $S_m(\omega)$ as the Fourier transform of $s_m(n)$, the Fourier transform of $x_m(n)$ is

$$X_m(\omega) = S_m(\omega)\left(1 + a\mathrm{e}^{\mathrm{j}(\omega_{\mathrm{d}} m - \omega l)}\right). \tag{6}$$

Applying squared modulus to both sides of Eq. (6), the power spectrum of $x(n)$ is obtained as follows:

$$P_{xm}(\omega) = P_{sm}(\omega)\left(1 + a^2 + 2a\cos(\omega_{\mathrm{d}} m - \omega l)\right), \tag{7}$$

whose logarithm can be represented as

$$\log\left(P_{xm}(\omega)\right) = \log\left(P_{sm}(\omega)\right) + \log\left(1 + a^2 + 2a\cos(\omega_{\mathrm{d}} m - \omega l)\right). \tag{8}$$

In PCL radar systems, the modulus of the moving target echo, a, is much smaller than unity (i.e., $|a| \ll 1$). Applying the log series expansion to the second term of the right side of Eq. (8), and ignoring the terms with a higher order of a and the constant, we obtain

$$\log\left(P_{xm}(\omega)\right) = \log\left(P_{sm}(\omega)\right) + 2a\cos(\omega_{\mathrm{d}} m - \omega l) - a^2\cos(2\omega_{\mathrm{d}} m - 2\omega l). \tag{9}$$

By applying the inverse Fourier transform, the power cepstrum can be obtained as follows:

$$\begin{aligned} F^{-1}\left\{\log\left(P_{xm}(\omega)\right)\right\} = {} & F^{-1}\left\{\log\left(P_{sm}(\omega)\right)\right\} \\ & + a[\delta(n-l)\mathrm{e}^{\mathrm{j}\omega_{\mathrm{d}} m} + \delta(n+l)\mathrm{e}^{-\mathrm{j}\omega_{\mathrm{d}} m}] \\ & - 0.5a^2\delta(n-2l)\mathrm{e}^{\mathrm{j}2\omega_{\mathrm{d}} m} - 0.5a^2\delta(n+2l)\mathrm{e}^{-\mathrm{j}2\omega_{\mathrm{d}} m}. \end{aligned} \tag{10}$$

It can be seen from the above expression that there is a phase rotation on the δ function, compared with that of the static target. The phase is closely related to the Doppler frequency and the starting time of the radar data.

3.3 DFT for the detection matrix

After calculating the power cepstrum of each data segment, the range information is obvious. However, the Doppler information is undetectable. Considering the relationship between the phase and the starting time of each data segment, we rewrite Eq. (10) as follows:

$$\begin{aligned} u_x(n,m) = {} & u_s(n,m) + a\left(\delta(n-l)\mathrm{e}^{\mathrm{j}\omega_{\mathrm{d}} m} + \delta(n+l)\mathrm{e}^{-\mathrm{j}\omega_{\mathrm{d}} m}\right) \\ & - 0.5a^2\delta(n-2l)\mathrm{e}^{\mathrm{j}2\omega_{\mathrm{d}} m} - 0.5a^2\delta(n+2l)\mathrm{e}^{-\mathrm{j}2\omega_{\mathrm{d}} m}, \end{aligned} \tag{11}$$

where $u_x(n, m)=F^{-1}\{\log(P_{xm}(\omega))\}$ and $u_s(n, m)=F^{-1}\{\log(P_{sm}(\omega))\}$.

Applying the Fourier transform in the slow time dimension to Eq. (11), we obtain

$$\begin{aligned} U_X(n,\omega) = {} & U_S(n,\omega) + a\delta(n-l)\delta(\omega-\omega_{\mathrm{d}}) \\ & + a\delta(n+l)\delta(\omega+\omega_{\mathrm{d}}) - 0.5a^2\delta(n-2l)\delta(\omega-2\omega_{\mathrm{d}}) \\ & - 0.5a^2\delta(n+2l)\delta(\omega+2\omega_{\mathrm{d}}). \end{aligned} \tag{12}$$

We can see from Eq. (12) that there are four peaks at points (l, ω_d), ($2l$, $2\omega_d$), ($-l$, $-\omega_d$), and ($-2l$, $-2\omega_d$). The peak at (l, ω_d) is the true peak, and the other peaks are side peaks, which result from the higher terms of the expansion of the log series. The position of the true peak denotes the delay and the Doppler frequency of the moving target. So, we can detect the moving targets by detecting the positions of the peaks in the detection matrix surface, and obtain their power by the amplitudes of the peaks.

3.4 Simulation results

The simulation throughout this article is on the background of the PCL radar systems. For simplicity, we use the complex Gaussian random process as the transmit signal for simulations, with a 9 MHz sampling rate, which is the same as that used in our real data system. A composited signal containing the reference signal and a single moving target's echo is constructed. The amplitude of the reference signal is normalized to unity, the amplitude a of the echo is 0.2, the Doppler frequency is 0.5 kHz, and the bistatic range is 13.366 km.

The simulation results of the CEPMTD algorithm are illustrated in Fig. 5, showing the results corresponding to Fig. 4. Fig. 5a shows the detection matrix after applying the power cepstrum in the fast time dimension. The target has already emerged in the matrix surface. However, the peaks exist along the entire slow time dimension. To obtain the Doppler information of the target and the larger accumulated gain of the target peak, DFT should be applied to the slow time dimension. After that, the results contain the range information and Doppler information of the targets (Fig. 5b). In Fig. 5b, the negative range is meaningless, and the average of the surface floor declines along the range. The peak at zero range in Fig. 5a is the power cepstrum of the reference signal in the composited signal, while the peak at zero range and zero Doppler in Fig. 5b is the moving target detection result of the reference signal in the composited signal. For clarity, we present only the interesting part of each detection matrix in the following simulation and experimental results, and its surface floor is compensated to be flat.

To compare the detection performances of the CEPMTD algorithm and radar CAF, we present the results of radar CAF in Fig. 6. The total integration time is the same when the improved CEPMTD algorithm is compared with CAF. The detection results in Figs. 5b and 6 show that the Doppler frequency and range detection precision of the CEPMTD algorithm are the same as those of the radar CAF. The PSL of the peak in Fig. 5b and Fig. 6 is 43.2 and 50.1 dB, respectively. The definition of PSL is the peaks' amplitudes subtracting the local average of the detection surface floor. The definition of the local average at each point is the average in the scope of a rectangle, whose center is this point. The size of the rectangle is an empirical value. When the detection matrix surface is flat, the size can be larger, and vice versa. It can be concluded that the detection capability of the CEPMTD algorithm is inferior to that of the radar CAF.

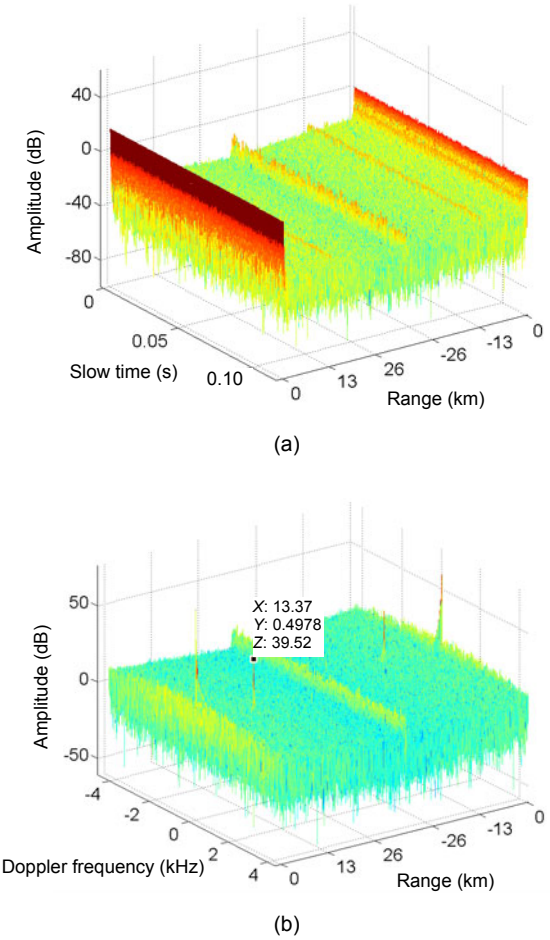

Fig. 5 Target detection results using the CEPMTD algorithm

(a) Detection matrix after applying the power cepstrum in the fast time dimension; (b) Detection matrix after applying DFT in the slow time dimension

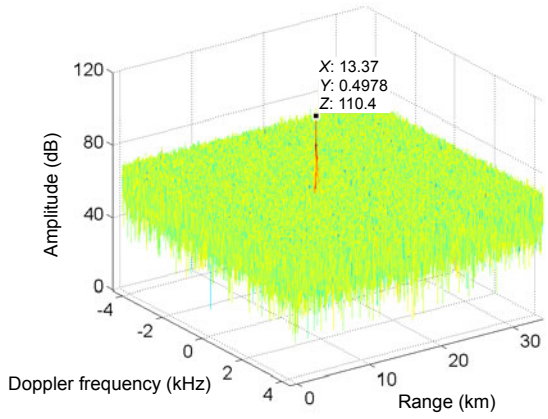

Fig. 6 Target detection results using the radar cross ambiguity function

4 Improved CEPMTD algorithm

4.1 Principle of the improved CEPMTD algorithm

In Section 3, the performance of the CEPMTD algorithm is compared with that of the radar CAF, which reveals that the former is inferior to the latter. In this section, an improved CEPMTD algorithm is proposed. The principle of this improved algorithm is to implement the CEPMTD algorithm many times and coherently add the results together.

Let P be the times of implementing CEPMTD. The steps of this improved algorithm can be summarized as follows:

Step 1: The composited signal is constructed by reference signal and moving target echo signal, which can be represented as

$$x_{mi}(n)=s_m(n)+as_m(n-l-i\cdot l_\mathrm{d})\mathrm{e}^{\mathrm{j}\omega_\mathrm{d}m}, \quad (13)$$

where i denotes the cycle number, and $i\cdot l_\mathrm{d}$ stands for the time shift for the moving target echo signal.

Step 2: Implementing the CEPMTD algorithm to $x_{mi}(n)$, the result is

$$\begin{aligned}U_{\mathrm{XI}}(n,\omega)=&U_S(n,\omega)+a\delta(n-l-i\cdot l_\mathrm{d})\delta(\omega-\omega_\mathrm{d})\\&+a\delta(n+l+i\cdot l_\mathrm{d})\delta(\omega+\omega_\mathrm{d})\\&-0.5a^2\delta(n-2l-2i\cdot l_\mathrm{d})\delta(\omega-2\omega_\mathrm{d})\\&-0.5a^2\delta(n+2l+2i\cdot l_\mathrm{d})\delta(\omega+2\omega_\mathrm{d}).\end{aligned} \quad (14)$$

Step 3: Giving $U_{\mathrm{XI}}(n, \omega)$ a time shift of $-i\cdot l_\mathrm{d}$, $U_{\mathrm{XID}}(n, \omega)$ can be obtained as

$$\begin{aligned}U_{\mathrm{XID}}(n,\omega)=&U_{\mathrm{XI}}(n+i\cdot l_\mathrm{d},\omega)\\=&U_S(n+i\cdot l_\mathrm{d},\omega)+a\delta(n-l)\delta(\omega-\omega_\mathrm{d})\\&+a\delta(n+l+2i\cdot l_\mathrm{d})\delta(\omega+\omega_\mathrm{d})\\&-0.5a^2\delta(n-2l-i\cdot l_\mathrm{d})\delta(\omega-2\omega_\mathrm{d})\\&-0.5a^2\delta(n+2l+3i\cdot l_\mathrm{d})\delta(\omega+2\omega_\mathrm{d}).\end{aligned} \quad (15)$$

Step 4: If i is equal to P, jump to step 5; otherwise, jump to step 1.

Step 5: Sum all $U_{\mathrm{XID}}(n, \omega)$ up:

$$\begin{aligned}U(n,\omega)=&\sum_{i=0}^{P-1}U_{\mathrm{XID}}(n,\omega)\\=&\sum_{i=0}^{P-1}U_S(n+i\cdot l_\mathrm{d},\omega)+Pa\delta(n-l)\delta(\omega-\omega_\mathrm{d})\\&+a\sum_{i=0}^{P-1}\delta(n+l+2i\cdot l_\mathrm{d})\delta(\omega+\omega_\mathrm{d})\\&-0.5a^2\sum_{i=0}^{P-1}\delta(n-2l-i\cdot l_\mathrm{d})\delta(\omega-2\omega_\mathrm{d})\\&-0.5a^2\sum_{i=0}^{P-1}\delta(n+2l+3i\cdot l_\mathrm{d})\delta(\omega+2\omega_\mathrm{d}).\end{aligned} \quad (16)$$

It can be seen from Eq. (16) that the true peak of the target at (l, ω_d) becomes P times as large as the result of the CEPMTD algorithm. That is, the true peak can be coherently added. However, the other terms of Eq. (16) cannot be coherently added. So, we can improve the performance of the CEPMTD algorithm by sacrificing the computation time. Thus, the performance of the improved CEPMTD algorithm can theoretically exceed that of the radar CAF when there is no noise in the radar data.

4.2 Simulation of improved CEPMTD

Fig. 7 shows the simulation results of the improved CEPMTD algorithm. Fig. 7a shows the results under P=10, while Fig. 7b shows the results under P=100. The PSLs in Figs. 7a and 7b are 52.3 and 56.5 dB, respectively. Comparing Fig. 5b with Fig. 7a, the PSL in the former is about 9.1 dB less than the latter. The PSL in Fig. 7b is 4.2 dB more than that in

Fig. 7a. Compared with Fig. 6, the detection performance of the improved CEPMTD algorithm is 6.4 dB better than that of radar CAF when P=100.

The improved CEPMTD algorithm can reduce the level of the correlation sidelobes generated by the signal itself, which is confirmed by Eq. (16). However, for the noise level resulting from the noise component of the received signal, the detection performances of the improved CEPMTD algorithm and the radar CAF are the same. When the SNR is −25 dB, the detection results are as shown in Fig. 8. Fig. 8a shows the Doppler profiles of the radar CAF, while Fig. 8b shows the results of the improved CEPMTD. The PSLs of the target in Figs. 8a and 8b are 43.24 and 42.88 dB, respectively. So, the detection performance of the improved CEPMTD is approximately equal to that of the radar CAF.

5 Experimental results

5.1 Measurement and data processing

We use the real data received by a PCL radar prototype to verify the improved CEPMTD algorithm proposed in Section 4. This system operates on the ultra high frequency (UHF) band with a tunable center frequency and a tunable bandwidth. The digital television terrestrial broadcasting (DTTB) signal of a single-carrier mode without dual-pilots (Li *et al.*, 2012) is received from the DTTB transmitter with

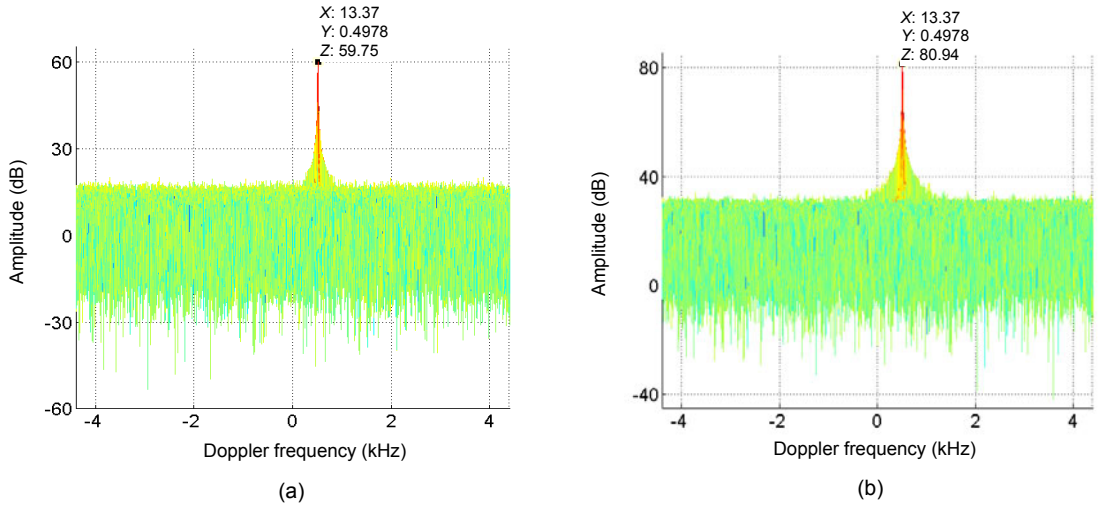

Fig. 7 Simulation results of the improved CEPMTD algorithm: (a) P=10; (b) P=100

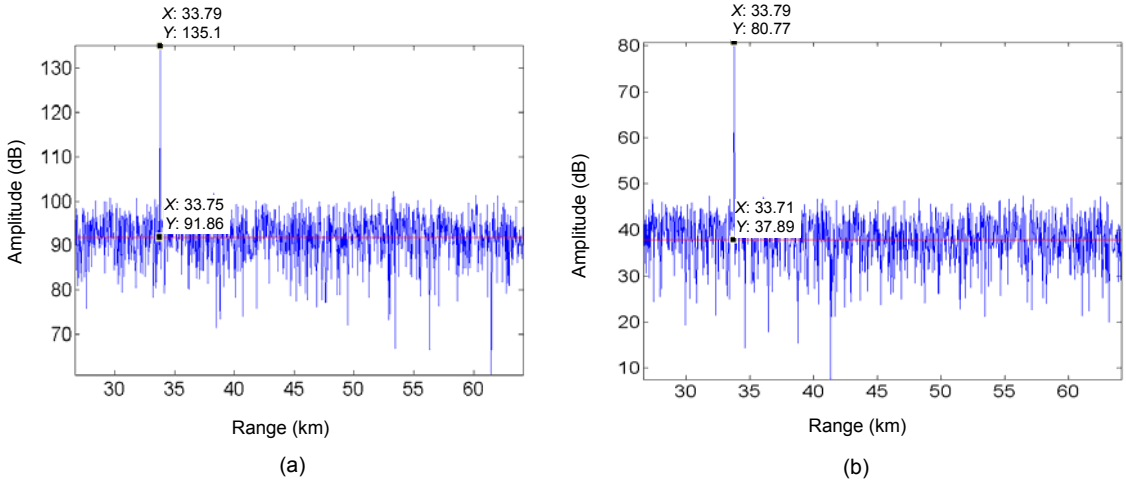

Fig. 8 Results of the Doppler profiles of radar CAF (a) and the improved CEPMTD algorithm (b)

33 channels on China Central Television, whose bandwidth is 8 MHz. The band-pass sampling rate is 33 MHz and after the digital down converter (DDC), the base band sampling rate is 9 MHz.

The block diagram of the overall signal processing operation is illustrated in Fig. 9. The reference signal and echo signal are received by reference and surveillance channels, respectively. Generally, the echo signal is received in the background of the direct path and multipath interferences, whose existence raises many problems to the detection of the moving targets, such as masking weak targets and emerging false alarms. So, the direct path and multipath interferences must be cancelled (Li *et al.*, 2013) before the subsequent processing of incorporating composited signal construction and moving target detection. Then we construct the composited signal with the reference signal and echo signal. Finally, the improved CEPMTD algorithm is implemented.

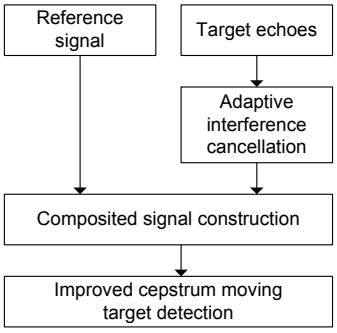

Fig. 9 Block diagram of the overall PCL radar signal processing operation

5.2 Target detection and tracking results

The results of target detection and tracking are presented in this subsection. The measurement campaign is conducted in the suburbs of Beijing city. The main targets for observation are civil aircrafts.

To illustrate the detection performance of the improved CEPMTD algorithm, multiple target trajectories are presented in Fig. 10. There are five target trajectories in Fig. 10a, which are detected at different times on the same day. We put the detection results together for evaluating the performance of the method more adequately. Each target is tracked for about 30 s. Fig. 10b shows the target tracks obtained from the Automatic Dependent Surveillance-Broadcast (ADS-B) receiver (Malanowski *et al.*, 2014) converted to the bistatic range-Doppler coordinates (R-D plane). It can be seen from Figs. 10a and 10b that targets 2, 3, and 5

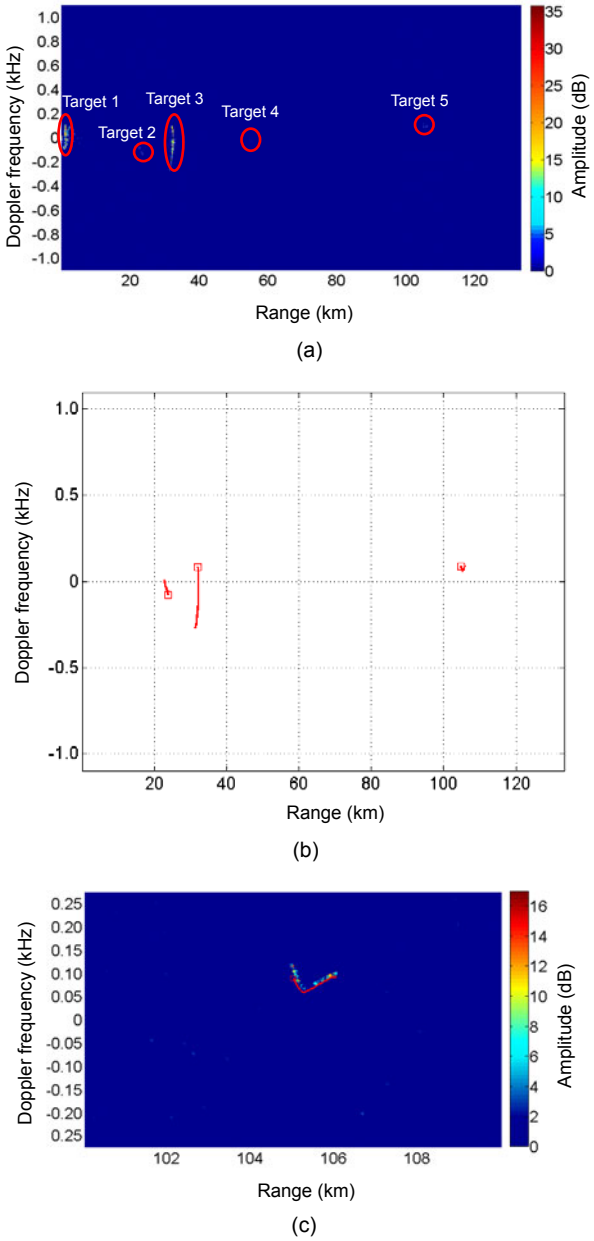

Fig. 10 Target tracks of multiple moving targets

(a) Moving target tracks by the improved CEPMTD algorithm; (b) Target tracks obtained from the ADS-B receiver (the squares denote the trajectory directions); (c) Detailed view of target 5 (the bright spots denote the detection results by the improved CEPMTD algorithm, and the red line denotes the target trajectory obtained from the ADS-B receiver). References to color refer to the online version of this figure

are confirmed by the ADS-B receiver, while targets 1 and 4 are not. Target 1 can be automobiles at a short range.

Fig. 10c shows the detailed view of target 5 with the ADS-B result as a reference. It can be seen that the detection results by the improved CEPMTD algorithm are confirmed by the results obtained from the ADS-B receiver, which shows that the improved CEPMTD algorithm can be successfully used in detecting moving targets in real PCL radar systems.

In Fig. 10, target 3 has a long trajectory and high SNR. The screenshot of the interface of the ADS-B receiver system is shown in Fig. 11, in which the trajectory of target 3 is shown in the polar coordinates.

The lengths of the used radar data of the radar CAF and the improved CEPMTD algorithm are the same. The detection results for target 3 using the radar CAF and the improved CEPMTD algorithm are shown in Figs. 12a and 12b (see the next page), respectively. It can be seen that the output of the improved CEPMTD algorithm is an R-D plane, which is the same as that of the radar CAF. Due to different algorithms being used, the amplitudes in Figs. 12a and 12b are different. However, there is a positive correlation between the PSL and the target echo's power. For comparison of the improved CEPMTD algorithm and the radar CAF, the Doppler profiles of the Doppler units, to which target 3 in Figs. 12a and 12b belongs are shown in Figs. 12c and 12d, respectively. In Fig. 12c, the amplitude of target 3 is 210.2 dB and the mean of the floor is 167.8 dB, and thus the PSL is 42.4 dB. In Fig. 12d, the amplitude of target 3 is 72.69 dB and the mean of the floor is 28.66 dB, and thus the PSL is 44.03 dB, which is 1.63 dB higher than that of the radar CAF. To more clearly illustrate our findings, we list the detection results in Table 1. It is observed that the detection performance of the improved CEPMTD algorithm is slightly better than that of the radar CAF in real radar data processing. This is because there is still the residual of the clutters in the real radar data after clutter removal.

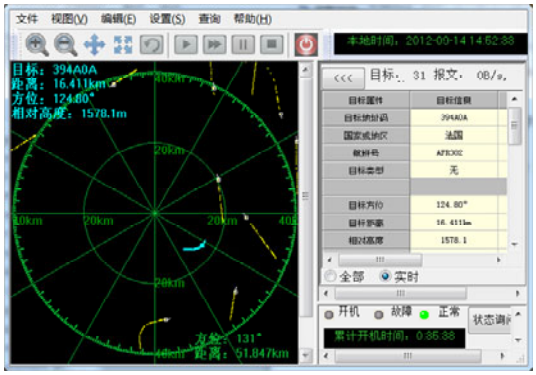

Fig. 11 The screenshot of the interface of the ADS-B receiver system (in Chinese)
The shaded area is the PCL radar system's surveillance area. The origin of the polar coordinates is the point of the PCL radar receiver

6 Conclusions

This paper presents a novel moving target detection algorithm based on cepstrum techniques for PCL radar systems, named CEPMTD. The classical moving target detection algorithm is the radar CAF, obtaining the range information and the Doppler information of moving targets by detecting the peak position in the output matrix of CAF. Being the same as radar CAF, the CEPMTD algorithm can produce a detection matrix, containing the range information and Doppler information. The resolution of the range and the Doppler frequency of the CEPMTD algorithm are the same as their counterparts of the radar CAF.

Based on the proposed CEPMTD algorithm, an improved CEPMTD algorithm is proposed to improve the detection capacity. Different composited signals are constructed by changing the relative time shift of the same reference signals and target echoes. Implementing the CEPMTD algorithm to each composited signal, all outputs of the CEPMTD algorithm

Table 1 Detection results of the radar CAF and improved CEPMTD algorithm

Algorithm	Integration time (s)	Doppler interval (kHz)	Range interval (km)	Target peak amplitude (dB)	Noise floor (dB)	PSL (dB)
Radar CAF	1	(−1, 1)	(27, 45)	210.20	167.80	42.40
Improved CEPMTD (a=1, P=100)	1	(−1, 1)	(27, 45)	72.69	28.66	44.03

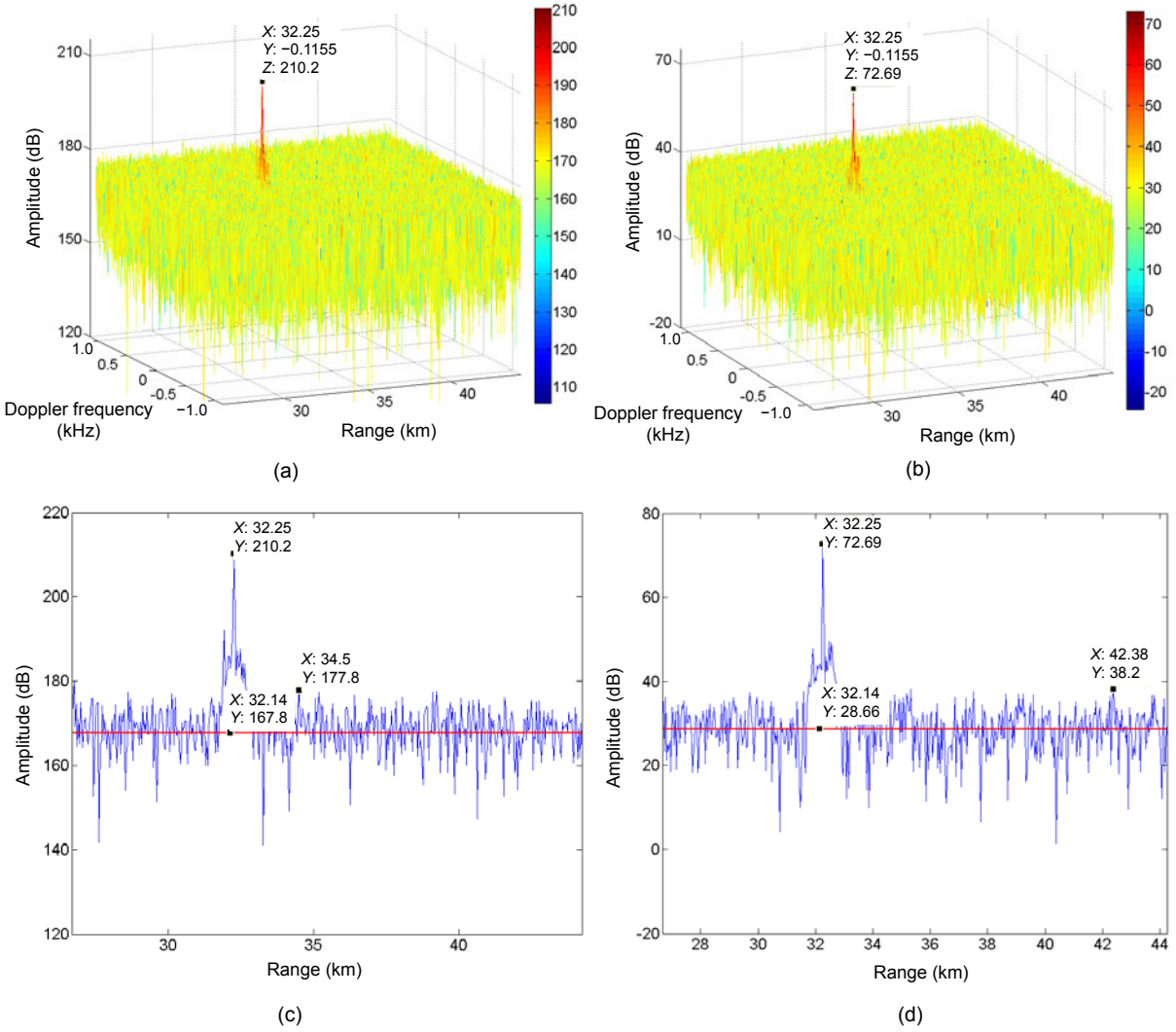

Fig. 12 Detection results for target 3

(a) Radar CAF results; (b) Improved CEPMTD algorithm results; (c) Doppler profile of radar CAF results; (d) Doppler profile of the improved CEPMTD algorithm results. The peaks' positions denote the targets' range and Doppler information

are summed up with the same time shift. The target's peak can be coherently added, while the sidelobes are added incoherently. Theoretical analyses show that the detection performance of the improved CEPMTD algorithm can exceed that of the radar CAF. This algorithm has been validated by simulations and experiments. The simulation results show that the PSL of the target peak detected by the improved CEPMTD algorithm when P=100, is 6.4 dB better than that by the radar CAF. In experimental results, five target trajectories have been presented. Three of them are confirmed by the ADS-B receiver. The experimental results show that the detection performance of the improved CEPMTD is 1.63 dB better than that of the radar CAF when P=100, which results from the residual of the clutters in the real radar data after clutter removal.

The improved CEPMTD algorithm can also be applied to moving target detection for other detection systems. It is certain that we have not seen the end of the applications of the improved CEPMTD algorithm.

References

Andric, M.S., Bujakovic, D.M., Bondzulic, B.P., *et al.*, 2011. Cepstrum-based analysis of radar Doppler signals. Proc. 10th Int. Conf. on Telecommunication in Modern Satellite Cable and Broadcasting Services, p.575-578. [doi:10.1109/TELSKS.2011.6143180]

Axelsson, S.R.J., 2004. Noise radar using random phase and frequency modulation. *IEEE Trans. Geosci. Remote Sens.*, **42**(11):2370-2384. [doi:10.1109/TGRS.2004.834589]

Bogert, B.P., Healy, M.J.R., Tukey, J.W., 1963. The quefrency analysis of time series for echoes: cepstrum, pseudo-autocovariance, cross-cepstrum and saphe cracking. Proc. Symp. on Time Series Analysis, p.209-243.

Cherniakov, M., 2008. Bistatic Radars: Emerging Technology. John Wiley & Sons, Inc., UK.

Hansson-Sandsten, M., Axmon, J., 2007. Multiple-window cepstrum analysis for estimation of periodicity. *IEEE Trans. Signal Process.*, **55**(2):474-481. [doi:10.1109/TSP.2006.885759]

Kemerait, R., Childers, D.G., 1972. Signal detection and extraction by cepstrum techniques. *IEEE Trans. Inform. Theory*, **18**(6):745-759. [doi:10.1109/TIT.1972.1054926]

Kim, H.K., Rose, R.C., 2003. Cepstrum-domain acoustic feature compensation based on decomposition of speech and noise for ASR in noisy environments. *IEEE Trans. Speech Audio Process.*, **11**(5):435-446. [doi:10.1109/TSA.2003.815515]

Kim, H.K., Rose, R.C., 2009. Cepstrum-domain model combination based on decomposition of speech and noise using MMSE-LSA for ASR in noisy environments. *IEEE Trans. Audio Speech Lang. Process.*, **17**(4):704-713. [doi:10.1109/TASL.2008.2012319]

Li, J., Lu, X., Zhao, Y., 2012. A novel algorithm for side peaks suppression of ambiguity function for passive radar based on Chinese DTTB signal. *J. Electron. (China)*, **29**(6):485-492. [doi:10.1007/s11767-012-0912-x]

Li, J., Zhao, Y., Lu, X., 2013. The impact of step selection in NLMS algorithm on low velocity target detecting for passive radar. Proc. IET Int. Radar Conf. [doi:10.1049/cp.2013.0359]

Malanowski, M., Kulpa, K., Kulpa, J., *et al.*, 2014. Analysis of detection range of FM-based passive radar. *IET Radar Sonar Navig.*, **8**(2):153-159. [doi:10.1049/iet-rsn.2013.0185]

Noll, A.M., 1964. Short-time spectrum and "Cepstrum" techniques for vocal-pitch detection. *J. Acoust. Soc. Am.*, **36**(2):296-302. [doi:10.1121/1.1918949]

Noll, A.M., 1967. Cepstrum pitch determination. *J. Acoust. Soc. Am.*, **41**(2):293-309. [doi:10.1121/1.1910339]

Olivadese, D., Giusti, E., Petri, D., *et al.*, 2013. Passive ISAR with DVB-T signals. *IEEE Trans. Geosci. Remote Sens.*, **51**(8):4508-4517. [doi:10.1109/TGRS.2012.2236339]

Oppenheim, A.V., 1965. Superposition in a Class of Nonlinear Systems. PhD Thesis, MIT Research Laboratory of Electronics, Cambridge, USA.

Oppenheim, A.V., Schafer, R.W., 2004. From frequency to quefrency: a history of the cepstrum. *IEEE Signal Process. Mag.*, **21**(5):95-106. [doi:10.1109/MSP.2004.1328092]

Palmer, J.E., Harms, H.A., Searle, S.J., *et al.*, 2013. DVB-T passive radar signal processing. *IEEE Trans. Signal Process.*, **61**(8):2116-2126. [doi:10.1109/TSP.2012.2236324]

Schafer, R.W., 1969. Echo Removal by Discrete Generalized Linear Filtering. Technical Report, MIT Research Laboratory of Electronics, Cambridge, USA.

Sinsky, A.I., Wang, C., 1974. Standardization of the definition of the radar ambiguity function. *IEEE Trans. Aerosp. Electron. Syst.*, **AES-10**(4):532-533. [doi:10.1109/TAES.1974.307831]

Stoffa, P.L., Buhl, P., Bryan, G.M., 1974. The application of homomorphic deconvolution to shallow-water marine seismology—Part I: models. *Geophysics*, **39**(4):401-416. [doi:10.1190/1.1440438]

Thomas, J.M., Griffiths, H.D., Baker, C.J., 2006. Ambiguity function analysis of digital radio mondiale signals for HF passive bistatic radar. *Electron. Lett.*, **42**(25):1482-1483. [doi:10.1049/el:20062896]

Tsai, W.H., Lin, H.P., 2011. Background music removal based on cepstrum transformation for popular singer identification. *IEEE Trans. Audio Speech Lang. Process.*, **19**(5):1196-1205. [doi:10.1109/TASL.2010.2087752]

Ulrych, T.J., 1971. Application of homomorphic deconvolution to seismology. *Geophysics*, **36**(4):650-660. [doi:10.1190/1.1440202]

Yan, H., Shen, G., Zetik, R., *et al.*, 2013. Ultra-wideband MIMO ambiguity function and its factorability. *IEEE Trans. Geosci. Remote Sens.*, **51**(1):504-519. [doi:10.1109/TGRS.2012.2201486]